2008-12

Inferring the Pattern of the Oceanic Meridional Transport from the Air-Sea Density Flux

Radko, Timour

Journal of Physical Oceanography, Volume 38, pp. 2722-2738, December 2008.
http://hdl.handle.net/10945/42129

Inferring the Pattern of the Oceanic Meridional Transport from the Air–Sea Density Flux

TIMOUR RADKO

Department of Oceanography, Naval Postgraduate School, Monterey, California

IGOR KAMENKOVICH*

Department of Atmospheric Sciences, University of Washington, Seattle, Washington

PIERRE-YVES DARE

Department of Oceanography, Naval Postgraduate School, Monterey, California

(Manuscript received 3 January 2007, in final form 30 April 2008)

ABSTRACT

An extension of Walin's water mass transformation analysis is proposed that would make it possible to assess the strength of the adiabatic along-isopycnal component of the meridional overturning circulation (MOC). It is hypothesized that the substantial fraction of the adiabatic MOC component can be attributed to the difference in subduction rates at the northern and southern outcrops of each density layer—the "push–pull" mechanism. The GCM-generated data are examined and it is shown that the push–pull mode accounts for approximately two-thirds of the isopycnal water mass transport in the global budget and dominates the Atlantic transport. Much of the difference between the actual interhemispheric flux and the push–pull mode can be ascribed to the influence of the Antarctic Circumpolar Current, characterized by the elevated (at least in the GCM) values of the diapycnal transport. When the diagnostic model is applied to observations, it is discovered that the reconstructed MOC is consistent, in terms of the magnitude and sense of overturning, with earlier observational and modeling studies. The findings support the notion that the dynamics of the meridional overturning are largely controlled by the adiabatic processes—time-mean and eddy-induced advection of buoyancy.

1. Introduction

One of the biggest uncertainties in the theory of the meridional overturning circulation (MOC)—and the subject of a vigorous ongoing debate—is associated with the relative importance of the interior mixing and adiabatic advection for its establishment and maintenance. The classical view (Robinson and Stommel 1959; Munk 1966; Welander 1986; Whitehead 1995) emphasizes the water mass transformation in the ocean interior, implicitly assigning it a critical role in maintenance of the meridional overturning. This idea was challenged by a number of studies, particularly by Wunsch and Ferrari (2004), who demonstrate that to reproduce overturning of realistic strength via diffusive mechanisms requires unrealistically high values of vertical mixing. Mechanical forcing by winds, on the other hand, appears to be an essential ingredient of the thermohaline system; neglecting the wind stress in multicentury simulations, for instance, leads to a complete shutdown of the conveyor belt circulation (Timmermann and Goosse 2004). These findings suggest that the interior diffusion may not be as critical for maintenance of the MOC as are adiabatic processes—wind forcing, advection, and eddy transfer. The latter proposition has gained considerable attention recently (Toggweiler and Samuels 1998; Gnanadesikan 1999; Marshall

* Current affiliation: Rosenstiel School of Marine and Atmospheric Science, University of Miami, Miami, Florida.

Corresponding author address: Timour Radko, Dept. of Oceanography, Naval Postgraduate School, Monterey, CA 93943.
E-mail: tradko@nps.edu

DOI: 10.1175/2008JPO3748.1

and Radko 2003; Radko 2007), but it requires independent and objective support.

Although the transformation of water masses is required to maintain steady-state overturning, a question arises whether the diabatic mixing plays a largely passive role or whether it can actively control the magnitude and pattern of the MOC. The answer to that may depend on a particular branch of the thermohaline circulation. Modern theory of the meridional overturning (e.g., Webb and Suginohara 2001; Boccaletti et al. 2005) identifies at least two distinct dynamic components of circulation: the shallow overturning cells in the main thermocline and deep circulation in the abyssal ocean. In the abyssal regions, shielded from the direct influence of wind, small-scale mixing processes are necessary to resupply the potential energy removed in the interior by the overturning and eddy-generating process (Wunsch and Ferrari 2004). On the other hand, dynamics of the strongly stratified central thermocline and the associated shallow overturning are controlled by the ventilation of water masses along the isopycnals that outcrop at the sea surface (Luyten et al. 1983). Winds provide energy for the meridional overturning, making it possible to maintain the circulation even in the absence of vertical diffusion below the mixed layer. Thus, the role of diapycnal mixing in the maintenance of the upper cell is questionable (Marshall et al. 2002). Attempts have been made to express the two views on general circulation—adiabatic and mixing driven—in terms of a unified theory (Salmon 1990; Samelson and Vallis 1997). These models advocate a concept of a two-thermocline ocean: the upper, largely adiabatic thermocline with isopycnals that outcrop in the subtropical gyre on top of the internal thermocline characterized by the advective–diffusive balance.

While the global characteristics of the oceanic overturning can be estimated from the air–sea fluxes (Trenberth and Caron 2001), the vertical pattern of the MOC is difficult to reconstruct from observations or models. All numerical modeling studies assume parameterizations of subgrid processes, the magnitude and functional dependencies of which are a significant source of uncertainty. Inverse databased models rely on sparse in situ measurements and allow only a crude description of the vertical structure of MOC (Sloyan and Rintoul 2000; Talley 2003). An alternative, conspicuously successful approach was proposed by Walin (1982), who related the integrated rates of water mass transformation at isopycnal surfaces to the air–sea buoyancy fluxes. Walin's technique was extended and applied to the Atlantic (Speer and Tziperman 1992; Marshall et al. 1999; Tandon and Zahariev 2001; Donners et al. 2005) and to the global ocean (Speer et al. 1995). The water mass transformation at a given buoyancy surface is, in turn, linked to the diapycnal volume flux (Tziperman 1986), which makes it possible to evaluate the diapycnal transport from the sea surface data.

A diagnostic of the isopycnal pole-to-pole component of the MOC from the sea surface data is more challenging. The movement along the isopycnal surfaces does not affect the density census of ocean water masses, and therefore the isopycnal flux is not directly linked to the integral measures of density forcing at the surface. In addition, it is now widely accepted that in the upper ocean the buoyancy transport by mesoscale eddies is often comparable in magnitude to the advection by the time-mean flow (e.g., Radko and Marshall 2004; Henning and Vallis 2004). As a result, the residual flow—the sum of the mean and eddy-induced circulations—is considerably different from the mean. Nevertheless, diagnostic models have been developed to infer the residual overturning circulation from the air–sea fluxes and surface buoyancy distribution (Speer et al. 2000; Karsten and Marshall 2002; Radko and Marshall 2006). These studies focused on the Southern Ocean, where predominantly zonal flow of the Antarctic Circumpolar Current (ACC) justified use of the simplified two-dimensional framework. A clear way of diagnosing the vertical structure of the global pole-to-pole MOC from the air–sea fluxes for complicated three-dimensional geometries of the isopycnals is still lacking.

Our work attempts to extend Walin's (1982) water mass transformation analysis, phrased here in terms of the residual circulation theory, to determine the isopycnal component of the meridional overturning. We argue that a large fraction of the isopycnal MOC can be attributed to the difference in the subduction rates at the northern and southern outcrops of each density layer; the subduction is, in turn, controlled by the sea surface density fluxes. Similar views were expressed in two-dimensional models of Marshall and Radko (2006) and Radko (2007), who relate the meridional transport of deep water to a combination of the isopycnal "pull" in the Southern Ocean and the isopycnal "push" from the north. Analysis of a numerical model in our paper confirms that the "push–pull" mode strongly affects the total isopycnal flux in all basins; in the Atlantic, the contribution of the push–pull mode is dominant. The simplicity of reconstruction of the push–pull mode from sea surface data, combined with its principal role in the interhemispheric transport, naturally leads to a transparent technique of inferring the isopycnal MOC component from the surface density flux. The new diagnostics, due to the limitations discussed in the text, are not a substitute for the explicit measures of isopycnal cir-

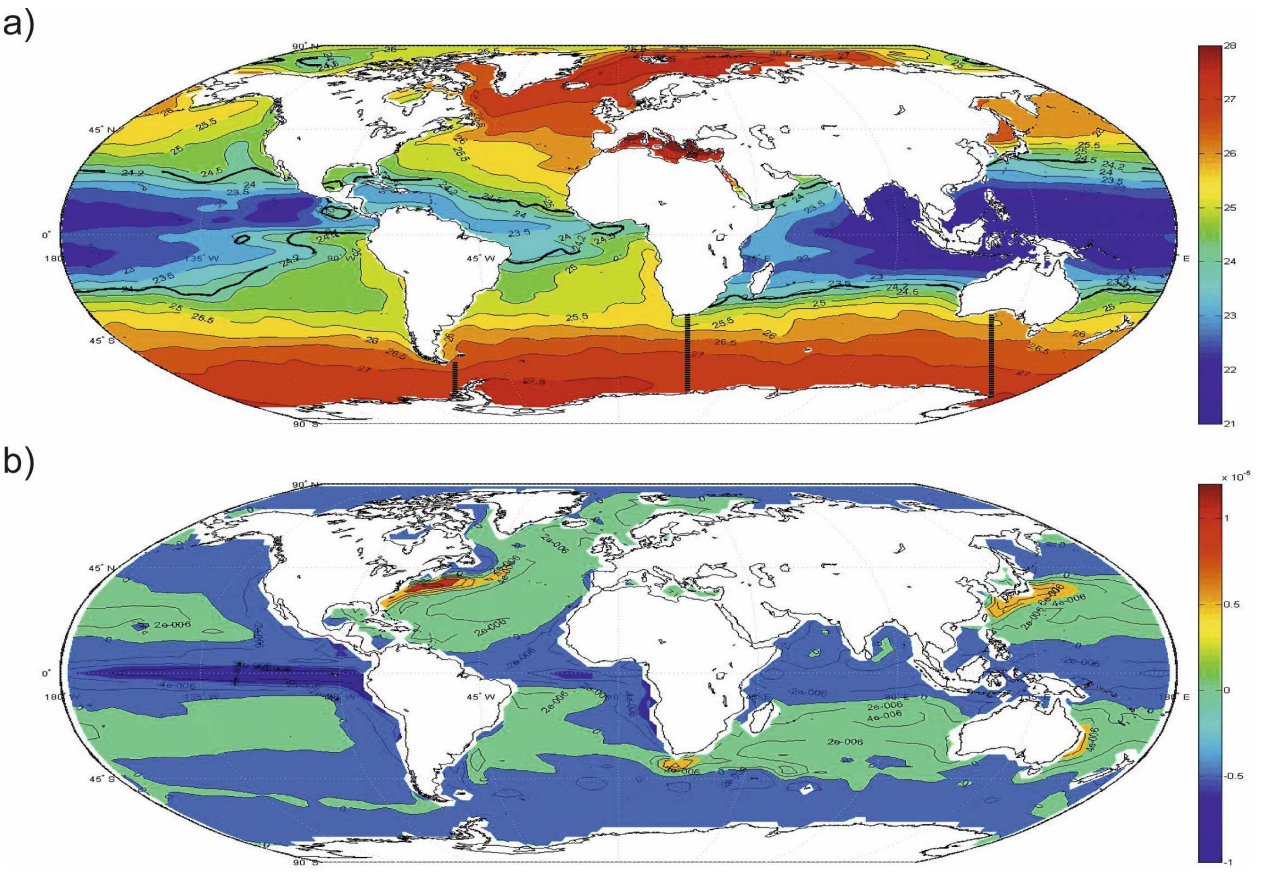

FIG. 1. Key observations used in the diagnostics of the MOC. (a) The surface density field from the Levitus climatology. Dashed lines indicate partitioning of the World Ocean into the individual basins. (b) The air–sea density flux based on the ECMWF reanalysis. The heavy solid curves indicate the lowest surface density contours (σ_0) included in the analysis.

culation based on direct measurements or inverse-model estimates. However, we believe that they can complement and extend the more conventional techniques and provide a simple method of predicting the response of MOC to changing atmospheric forcing.

The paper is set up as follows: in section 2, we develop a diagnostic framework that quantifies the along-isopycnal transport in each density layer from the air–sea fluxes and mixed layer density distribution. To gain confidence in the proposed technique, it is first tested on the GCM-generated data (section 3). The isopycnal MOC component is computed in two ways: (i) by using the diagnostic framework of section 2 to infer the push–pull mode from the mixed layer density and the air–sea density flux; and (ii) by evaluating it directly from the meridional velocity distribution in the model. A general agreement between the two estimates supports our physical picture of MOC as a largely adiabatic mode of circulation, whereas the differences indicate the importance of diapycnal fluxes for some density classes. In particular, the more detailed analysis in section 4 suggests that much of the difference between the actual transport and the inferred push–pull mode in deep layers can be attributed to the diapycnal fluxes in the Southern Ocean. The proposed diagnostics are applied to observed sea surface data in section 5. We summarize and conclude in section 6.

2. Formulation

Figure 1 presents observations of the key surface properties for the global ocean. In Fig. 1a, we plot the subsurface (40 m) potential density σ (referenced to the sea surface) from the Levitus climatology. Figure 1b shows the air–sea density flux (B) based on the European Centre for Medium-Range Weather Forecasts (ECMWF) reanalysis, conventionally defined as

$$B = -\frac{\alpha H}{C_p} + \beta\rho_0 \frac{(E - P)S}{1 - S}, \qquad (1)$$

where (α, β) are the expansion/contraction coefficients; ρ_0 is the density of water; H is the heat flux into the

ocean; S is salinity; E and P are the rates of evaporation and precipitation, respectively; and C_p is the specific heat capacity of seawater. Our objective is to utilize observations in Fig. 1 to reconstruct the pattern of the meridional overturning, globally and in the individual basins. For tractability reasons, our analysis will be confined to water masses with $\sigma > \sigma_0$, where σ_0 is the minimum value of potential density for which southern and northern outcrops of the isopycnal surfaces do not intersect throughout the year; the outcrop with $\sigma_0 = 24.2$ is indicated by the solid line in Fig. 1a.

a. Elements of Walin's water mass transformation theory

A remarkably simple framework for the analysis of the water mass transformation induced by the air–sea fluxes (B) was proposed by Walin (1982). Walin phrased the buoyancy budget of the volume bounded by two density surfaces σ and $\sigma + \Delta\sigma$ in terms of advective and diffusive fluxes:

$$A(\sigma) = F(\sigma) - \frac{dD(\sigma)}{d\sigma}, \tag{2}$$

where $A(\sigma)$ is the diapycnal advective volume flux, $D(\sigma)$ is the diapycnal diffusive flux, and

$$F(\sigma) = \frac{1}{\Delta\sigma}\int_{\delta S} B\, dx\, dy \tag{3}$$

is the air–sea transformation function; $\delta S = (dS/d\sigma)\Delta\sigma$ is the surface area between isopycnals σ and $\sigma + \Delta\sigma$ (see the schematic in Fig. 2).

The advective term in the original model (Walin 1982) did not explicitly include the eddy transfer; it represented either the steady flow or the instantaneous balances. However, Eq. (2) can be readily reinterpreted (e.g., Cerovečki and Marshall 2008) to include the eddy-induced "skew flux" (Andrews and McIntyre 1976)—the advection by the nondivergent velocity field $\mathbf{v}^*$ associated with mesoscale activity. Therefore, we conveniently redefine the diapycnal flux term as

$$A = \int_{\sigma} \mathbf{v}_{\text{res}} \cdot \mathbf{m}\, dS, \tag{4}$$

where the residual velocity $\mathbf{v}_{\text{res}} = \mathbf{v} + \mathbf{v}^*$ represents the advection of buoyancy and tracers by both time-mean velocity ($\mathbf{v}$) and adiabatic eddies ($\mathbf{v}^*$). The integration in (4) is carried over the area of the isopycnal surface σ (or a portion of it), and $\mathbf{m}$ is the unit vector normal to this surface. The nonskew eddy fluxes (the eddy flux component that is not be represented by $\mathbf{v}^*$ advection) are incorporated in the diffusive flux D in Eq. (2).

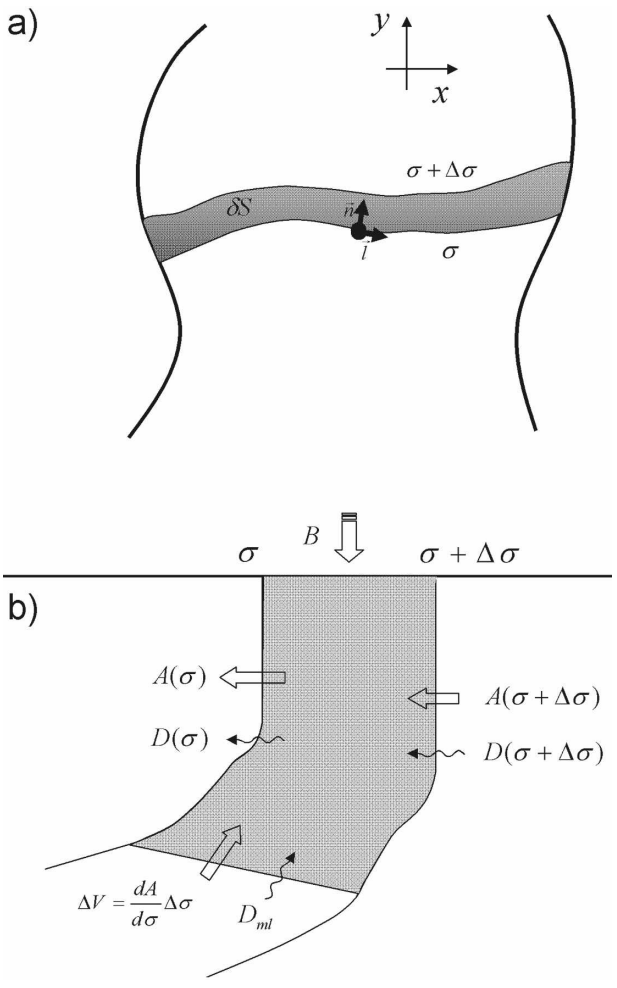

FIG. 2. Illustration of the diagnostic framework. We consider the volume and density budgets for the area bounded by two surface isopycnals σ and $\sigma + \Delta\sigma$. (a) Horizontal and (b) vertical sections.

b. Subduction rates

For our purpose, it is necessary to distinguish between the water mass transformation in the upper diabatic mixed layer and in the ocean interior. In the appendix, we offer a self-contained formulation for the budget of the mixed layer, the key result of which is

$$\Delta V = F(\sigma + \Delta\sigma) - F(\sigma), \tag{5}$$

where ΔV represents the volume flux of fluid abducted or subducted within the given density class $[\sigma\ \sigma + \Delta\sigma]$. Equation (5) can be physically interpreted in terms of Walin's (1982) model. It can be shown (Marshall 1997; Garrett and Tandon 1997; Radko 2007) that the lateral diffusive fluxes in the mixed layer are considerably less for large-scale budgets than the air–sea transformation term and that the vertical diffusive flux greatly reduces below the diabatic mixed layer. Therefore, the diffusive

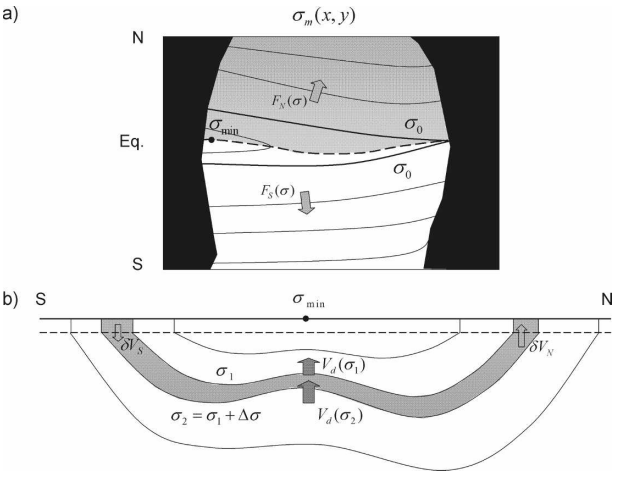

FIG. 3. Schematic of the density structure in a zonally bounded ocean. (a) Surface density distribution. For each value of $\sigma > \sigma_0$ there are two nonintersecting contours of surface density: one in the northern part (indicated by the gray shading) and one in the southern (not shaded). (b) The vertical meridional cross section of density. The volume flux entering the density layer bounded by the isopycnals σ_1 and σ_2 from the mixed layer ($\delta V_S + \delta V_N$) is balanced by the diapycnal flux $[V_d(\sigma_2) - V_d(\sigma_1)]$.

term D in (2) can be neglected, and the mixed layer buoyancy budget [see, e.g., Eq. (1.5) in Garrett et al. (1995)] can be locally approximated as $A \approx F$. Next, we recognize that the volume flux into the mixed layer from the interior (ΔV) is $(dA/d\sigma)\Delta\sigma$, and therefore $\Delta V \approx (dF/d\sigma)\Delta\sigma$, as in (5). The volume flux ΔV at the base of the "diabatic layer" h_m can be written as

$$\Delta V = \iint_{\delta S} W\, dx\, dy, \tag{6}$$

where

$$W = w_{\text{res}|z=-h_m} + (u_{\text{res}}, v_{\text{res}}) \cdot \nabla h_m$$

is the volume flux per unit area. We note that the definition of h_m from density field is not straightforward because the diabatic layer with elevated diapycnal mixing does not necessarily coincide with the actual homogeneous mixed layer (Marshall and Radko 2003).

c. Isopycnal and diapycnal advection

While the original Walin (1982) formulation involves the *total* transformation, in which the air–sea density fluxes in both hemispheres are grouped together, in our model it is essential to distinguish the water mass transformation in the Northern and Southern Hemispheres. As shown in the schematic diagram in Fig. 3, for each $\sigma > \sigma_0$, generally, there are two distinct values of $F \approx A$ corresponding to the southern and northern outcrops; these are denoted as $F_S(\sigma)$ and $F_N(\sigma)$, respectively. Because the residual circulation is assumed to be nondivergent, the flux (V_d) crossing the isopycnal σ in the ocean interior (see the schematic in Fig. 3b) is equal to the flux from the diabatic layer within the sea surface area, where $\sigma_m < \sigma$. The latter, in view of (5), reduces to

$$V_d(\sigma) = \iint_{\sigma' < \sigma} W\, dS = F_S(\sigma) + F_N(\sigma) \quad \text{for} \quad \sigma > \sigma_0\,. \tag{7}$$

The sign convention is such that V_d is positive (negative) for the upward (downward) integrated cross-isopycnal flux. We emphasize that the diapycnal flux V_a in (7) pertains only to the water mass transformation in the ocean *interior*.

Our next step—and the key strength of the proposed analysis—is to quantify the magnitude and pattern of the isopycnal pole-to-pole MOC component from surface data. We separately consider the Northern and Southern Hemispheres and in each case compute the residual volume flux entering (escaping) the interior into (from) the mixed layer. The highest value of the potential density that can be found in the mixed layer is denoted by $\sigma_{\max}$, and σ lies within the interval $\sigma_0 < \sigma < \sigma_{\max}$. For each hemisphere, we use (5) to express the net residual flux at the bottom of the mixed layer within a density range of $[\sigma, \sigma_{\max}]$ in terms of F as follows:

$$\begin{cases} V_N(\sigma) = \displaystyle\iint_{\substack{\sigma_{\max} < \sigma' < \sigma \\ \text{north}}} W\, dS = F_N(\sigma_{\max}) - F_N(\sigma), \\ V_S(\sigma) = \displaystyle\iint_{\substack{\sigma_{\max} < \sigma' < \sigma \\ \text{south}}} W\, dS = F_S(\sigma_{\max}) - F_S(\sigma). \end{cases} \tag{8}$$

Because the residual flow is nondivergent, the sum of all fluxes entering the interior volume bounded by the isopycnals $\sigma_{\max}$ and σ is zero (see the schematic in Fig. 3b):

$$V_d(\sigma) - V_d(\sigma_{\max}) + V_N(\sigma) + V_S(\sigma) = 0. \tag{9}$$

In the absence of any cross-isopycnal flows, Eq. (9) would reduce to $V_N(\sigma) = -V_S(\sigma)$, which is readily interpreted as a statement that all the water subducted in the Southern Hemisphere upwells in the Northern Hemisphere. In this case, the isopycnal flux throughout the density layer $[\sigma_{\max}, \sigma]$ is uniform and equal to $V_N(\sigma)$.

Of course, in reality there is a finite diapycnal flux across any isopycnal surface. Consequently, $V_N(\sigma)$ is

not equal to $-V_S(\sigma)$ and the isopycnal flux cannot be precisely determined from the surface conditions; the pole-to-pole MOC can be affected by the interior diabatic mixing. Therefore, an attempt is now made to isolate and quantify the MOC component that is entirely driven by the subduction/obduction from the mixed layer (V_S and V_N). We shall refer to this component as the push–pull mode: $V_a = V_a(V_S, V_N)$.

To arrive at a physically meaningful definition of the push–pull mode V_a, suppose that the response of the push–pull mode to the surface forcing can be linearized in the regime of interest:

$$V_a = aV_S + bV_N + c. \tag{10}$$

To specify the coefficients in (10), we invoke three arguments: (i) because a priori the two outcrops of each density layer are equally important in setting the average along-isopycnal flux, we insist that $a = -b$ in (10); (ii) in the limit of the symmetric ocean, in which the Northern Hemisphere is a mirror image of the Southern Hemisphere ($V_N = V_S$), we expect no interhemispheric transport, and therefore c is zero; and (iii) in the limit of the adiabatic ocean, isopycnal transport is uniform throughout the layer and $V_a = V_N = -V_S$. Drawing together (i)–(iii), we arrive at $a = 0.5$, $b = -0.5$, and $c = 0$ in (10), or

$$V_a(\sigma) = \frac{1}{2}[V_N(\sigma) - V_S(\sigma)]. \tag{11}$$

Equation (11) defines the push–pull MOC component by the average value between the downward volume flux at the base of the mixed layer in the Southern Hemisphere and the corresponding upward flux in the Northern Hemisphere. If an isopycnal surface outcrops in only one hemisphere (as isopycnals $28 < \sigma < 28.3$, which do not outcrop in the Northern Hemisphere), one can still use (11) provided that the subduction rate in the absence of outcrop is set to zero. While the definition (11) seems somewhat arbitrary at first, its application to the ocean general circulation model (OGCM)-generated data in section 3 indicates that the push–pull mode (11) is consistent, in terms of the general pattern and magnitude, with the actual interhemispheric transport.

Because the length of the surface density contours inevitably reduces to zero as density approaches its highest possible value ($\sigma_{\max}$), we anticipate that $F_N(\sigma_{\max}) \approx F_S(\sigma_{\max}) \approx 0$ in Eq. (8), and therefore (11), reduces to

$$V_a(\sigma) = \frac{1}{2}[F_S(\sigma) - F_N(\sigma)], \tag{12}$$

which can be readily evaluated from the available sea surface data.[1]

d. What fraction of the interhemispheric transport can be attributed to the push–pull mode?

The expressions in (11) and (12) attempt to quantify the transport component associated with the subduction at the outcrops of each density layer. It is therefore of interest to compare V_a with more direct measures of the isopycnal transport, such as the total cross-equatorial flux that we consider next.

Denoting the northward volume flux at the equator within the density layer $[\sigma_{\max}, \sigma]$ by $V_{\text{eq}}(\sigma)$, we balance the budgets of the southern and northern parts of the interior volume bounded by the isopycnals $\sigma_{\max}$ and σ as follows:

$$\begin{cases} V_N(\sigma) + V_d^N(\sigma) - V_d^N(\sigma_{\max}) - V_{\text{eq}}(\sigma) = 0, \\ V_S(\sigma) + V_d^S(\sigma) - V_d^S(\sigma_{\max}) + V_{\text{eq}}(\sigma) = 0, \end{cases} \tag{13}$$

where V_d^N (V_d^S) is the cross-isopycnal interior volume transport in the Northern (Southern) Hemisphere. Subtracting the two equations in (13) and using (11), we arrive at

$$V_{\text{eq}}(\sigma) = V_a(\sigma) + \frac{1}{2}\big[V_d^N(\sigma) - V_d^S(\sigma) + V_d^S(\sigma_{\max}) - V_d^N(\sigma_{\max})\big]. \tag{14}$$

Equation (14) implies that the difference between the push–pull mode and the actual transport is set by the term $V_{\text{diap}} = 0.5(V_d^N - V_d^S)$, representing the difference between the diapycnal fluxes in the Northern and Southern Hemispheres, and further reduces to zero for $\sigma \to \sigma_{\max}$. The relative difference between the push–pull mode and total transport is measured by

$$\delta = \frac{\text{rms}(V_d^N - V_d^S)}{2\text{rms}(V_{\text{eq}})}. \tag{15}$$

The subsequent analysis of the numerical model (section 3) indicates that δ is small, and therefore the push–pull mode accounts for a large fraction of the total interhemispheric transport.

[1] Note that σ in foregoing formulation exceeds σ_0 and, therefore, Eq. (12) cannot describe the overturning in the upper tropical thermocline, where $\sigma < \sigma_0$. However, the region corresponding to this density range occupies only a small fraction of the thermocline, with the maximum depth of 200 m and, therefore, its relative contribution to the overall overturning is expected to be of secondary importance.

3. Analysis of a numerical simulation

The method described in section 2 is now applied to the ocean state simulated in a GCM; the push–pull mode (V_a), computed from the air–sea density flux, is compared with the interhemispheric transport ($V_{\rm eq}$) directly derived from the GCM-simulated velocities. We diagnose the global overturning and then examine its Atlantic and Indo-Pacific components. The key strength of the GCM analysis is that the buoyancy fluxes, stratification, and velocity fields are both dynamically consistent and readily available.

a. Numerical model

The model (Kamenkovich 2005) is based on the Geophysical Fluid Dynamics Laboratory (GFDL) Modular Ocean Model version 3 (MOM3) code (Pacanowski and Griffies 1999). The horizontal resolution is 2° in longitude and latitude; there are 25 levels in the vertical with resolution increasing from 17 m at the surface layer to 510 m at the bottom; bathymetry of the model is derived from the Scripps topography. Vertical diffusivity varies from 0.25×10^{-4} m^2 s^{-1} at the surface to 1.0×10^{-4} m^2 s at the bottom, reflecting the increase of the vertical mixing in the deep ocean (Bryan and Lewis 1979) and its further intensification by rough bottom topography (Polzin et al. 1997). Heat and salt transports by the mesoscale eddies are parameterized by the Gent–McWilliams scheme (Gent and McWilliams 1990), and the *K*-profile parameterization scheme (Large et al. 1994) is used to represent turbulent mixing within a boundary layer. For the analysis, we use the 1990 simulation. The simulated surface density field is as realistic as can be expected in a coarse-resolution model (Fig. 4a), and the surface buoyancy fluxes (Fig. 4b) are quantitatively consistent with observations. Despite substantial errors in the equatorial and western boundary currents, attributed mainly to the coarse horizontal resolution, gross features of the meridional overturning circulation are simulated realistically. The maximum overturning in the North Atlantic is 18 Sv (1 Sv $\equiv 10^6$ m^3 s^{-1}), which is consistent with data-based estimates (Talley et al. 2003); a credible value of 6 Sv was obtained for the flux of the Antarctic Bottom Water.

b. Global circulation

The following analysis is limited to a density range $\sigma_0 < \sigma < \sigma_{\max}$, where $\sigma_{\max} = 28.0$ is the densest isopycnal that outcrops in both hemispheres and $\sigma_0 = 24.3$ is the lightest isopycnal with two nonintersecting outcrops (Fig. 4). Figure 5 presents the cross-equatorial volume flux $V_{\rm eq}$, indicated by the dashed curve, along with the push–pull mode V_a (solid curve); $V_{\rm eq}$ is calculated as the sum of the monthly mean Eulerian and eddy-induced velocities. It is apparent that overall, V_a in Fig. 5 is consistent with $V_{\rm eq}$ in terms of magnitude, sense of overturning, and the general pattern, particularly for relatively dense water masses ($\sigma > 25.5$). As in the actual GCM-simulated circulation, V_a represents three distinct branches of circulation: the upper waters,[2] northward-flowing thermocline and intermediate waters (IW), and southward return flow of the deep water. Of particular interest is the ability of the push–pull mode to represent the net northward transport in the main thermocline/IW class (see Table 1). The deep overturning is, however, stronger in the push–pull mode than in the GCM-simulated one. The main differences between V_a and $V_{\rm eq}$ are that (i) the lower boundary of the IW in V_a is at the lighter density than in $V_{\rm eq}$ and (ii) the transport of the upper waters in V_a is much stronger than in $V_{\rm eq}$.

As discussed in section 2d, the difference between V_a and $V_{\rm eq}$ is primarily caused by the diapycnal distortion term $V_{\rm diap} = 0.5(V_d^N - V_d^S)$. Both $V_{\rm eq}$ and $V_{\rm diap}$ were directly calculated from the model, and the ratio of their RMS values [see Eq. (15)] was found to be

$$\delta = 0.39. \tag{16}$$

This value is consistent with the differences of about 30% in Fig. 5 and supports our premise that the interhemispheric MOC is strongly influenced by the push–pull mechanism.

c. Partitioning of the global transport between the Atlantic and Indo-Pacific basins

To examine specifics of the individual ocean basins, we separately consider the Atlantic and Indo-Pacific components of the global overturning circulation. The water mass budget in these basins is affected by the inflow/outflow of the Antarctic Circumpolar Current (ACC), not taken into account in the theoretical model (section 2). However, our numerical results suggest that the imbalance of the ACC (Fig. 6) is rather weak and mostly affects the transport of dense deep-water masses. Therefore, the analysis of the push–pull mode in this section remains meaningful for densities lower than $\sigma \approx 27.3$.

In Fig. 7 we plot the cross-equatorial volume flux $V_{\rm eq}$ (dashed curve) and the push–pull mode V_a (solid curve)

[2] Note that because σ_0 is not the lowest density at the equator, $V_{\rm eq}$ includes only a portion of the transport of the upper-thermocline and surface waters.

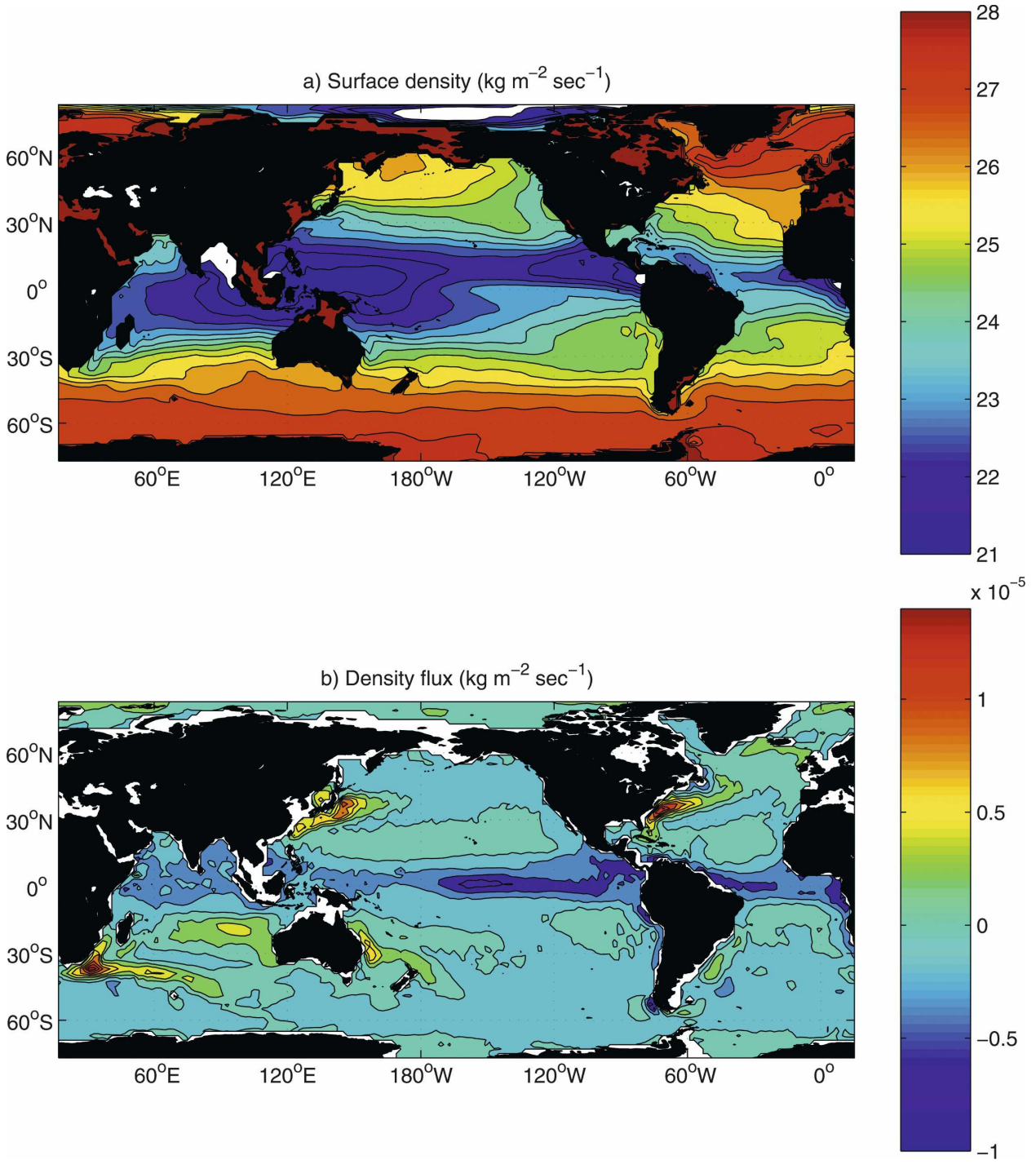

FIG. 4. GCM-simulated fields: (a) the surface density and (b) the air–sea density flux.

for the Atlantic. Three main branches of the GCM-simulated Atlantic overturning—circulation of the surface/thermocline waters, thermocline/IW, and deep return flow—are seen in both V_{eq} and V_a. For densities $26 < \sigma < 27.3$, the actual circulation V_{eq} and the push–pull mode V_a agree very closely. As in the global calculation (Fig. 5), the volume flux in the upper layers ($\sigma < 26.0$) diverges from the push–pull mode V_a. For deep layers ($\sigma > 27.3$), the southward return flow of the deep water is noticeably stronger in V_{eq} than in V_a. Overall, we find that in the Atlantic the push–pull mode comes closer to describing the net interhemi-

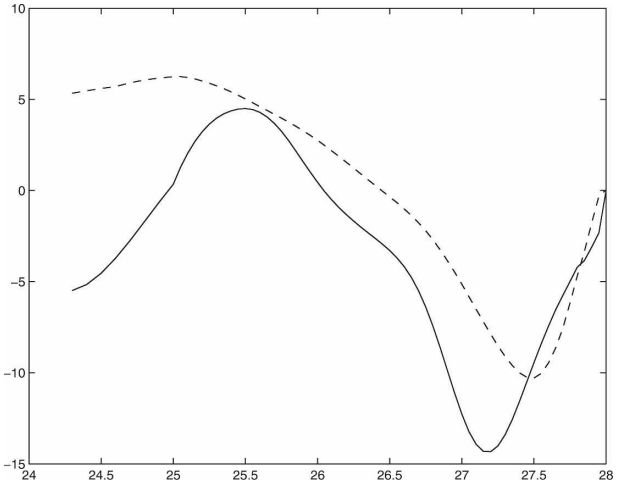

FIG. 5. The global overturning. The zonally integrated isopycnal volume flux (in Sv) between $\sigma_{max} = 28.0$ and σ is plotted as a function of σ. The dashed line shows the GCM-simulated values at the equator (V_{eq}); the solid line shows the push–pull mode V_a estimated from the surface density fluxes. Increase with σ corresponds to the northward transport.

spheric transport than in the global ocean (see Fig. 5). This feature can be rationalized by computing the relative amplitude of the diapycnal distortion term (15):

$$\delta_{Atl} = 0.27,$$

which is considerably less than the global value (16). It is perhaps not surprising that the push–pull mode is dominant in the Atlantic: here, the diapycnal fluxes in both hemispheres are weak (because of its small area) and their contribution to V_{diap} is partially cancelatory, whereas the isopycnal transport is substantial.

Next, we turn to the Indo-Pacific basin. The decision to combine the Indian and Pacific Oceans was made to avoid consideration of the influence of the Indonesian Throughflow. While there is still some qualitative similarity between V_a and V_{eq} (Fig. 8), the agreement between the two is by far worse than in the Atlantic. The actual and inferred rates of the isopycnal volume flux, measured by the slopes of the curves in Fig. 8, are consistent in the $25.0 < \sigma < 26.5$ range. However, the push–pull mode exaggerates the strength of MOC for $\sigma > 26.5$: both the northward transport of the thermocline/IW water and southward transport of the deep water are noticeably stronger than in V_{eq}. The lower boundary of the northward-flowing IW layer is at $\sigma > 27.2$, which is significantly shallower than in the actual GCM fields; this feature ultimately leads to a similar bias in the global overturning (Fig. 5). Overall, the visual inspection of Figs. 5, 7, 8 indicates that the major source of deviation of the global push–pull mode from the actual transport lies in the Indo-Pacific dynamics. Because of the large area and pronounced asymmetry of the Indo-Pacific basin with respect to the equator, the diapycnal distortion term V_{diap} becomes substantial (see section 2d), which ultimately leads to the difference between V_a and V_{eq}.

TABLE 1. Northward transport (Sv) of the thermocline water masses in the GCM. The estimates based on the actual interhemispheric transport (V_{eq}) and on the push–pull mode (V_a) are mutually consistent. The transport is calculated as a variation between minimum and maximum in V_{eq} and V_a.

	Global	Atlantic	Indo-Pacific
Cross-equatorial flux	16.5	7.4	9.2
Theory-based estimate	18.8	7.6	14.6

4. Influence of the Southern Ocean

The foregoing analysis motivates an inquiry into the causes of the diapycnal distortion $V_{diap} = 0.5(V_d^N - V_d^S)$—the term responsible (section 2d) for differences between the push–pull mode and actual transport. Here, V_{diap} reflects the asymmetry of the diapycnal fluxes in the two hemispheres, and one of the most asymmetric features of the World Ocean is the Antarctic Circumpolar Current in the Southern Hemisphere. The absence of meridional land barriers in the ACC results in distinct dynamical features that have no direct counterpart in the Northern Hemisphere. Accelerated by the westerly winds, the ACC circumnavigates the globe with the volume transport of 130–140 Sv. The ACC is characterized by enhanced eddy activity and by elevated diapycnal transfer (Olbers et al. 2004).

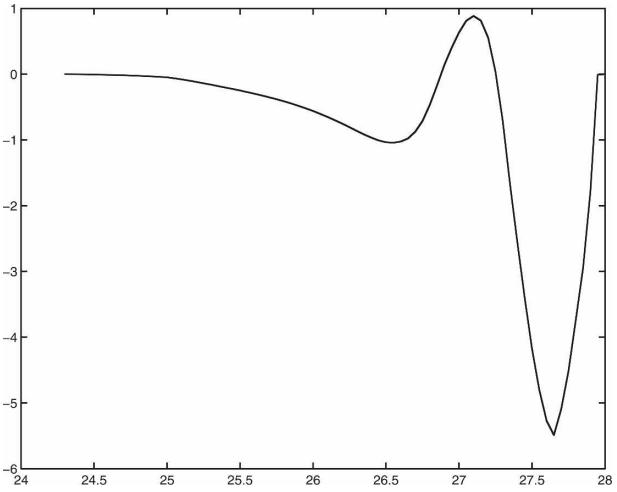

FIG. 6. Divergence of the zonal residual flow in the ACC between 64°W and 18°E.

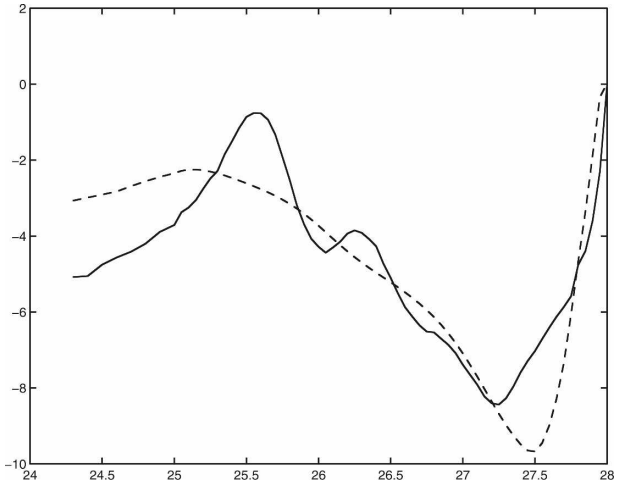

FIG. 7. Atlantic overturning. The zonally integrated isopycnal volume flux (in Sv) between $\sigma_{max} = 28.0$ and σ is plotted as a function of σ. The dashed line shows the GCM-simulated transport (V_{eq}) at the equator; the solid line shows the push–pull mode V_a estimated from the surface density fluxes. Increase in transport with σ corresponds to the northward flow.

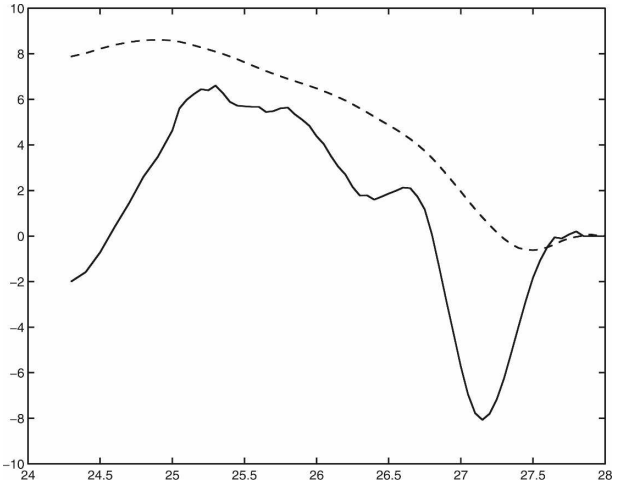

FIG. 8. Same as in Fig. 7, but for the Indo-Pacific basin.

In this section, we examine the possibility that the distortion term V_{diap} can be largely attributed to the water mass transformations within the ACC. In Fig. 9, we plot the oceanwide meridional transport at 30°S (V_{ACC}), the northern boundary of ACC, and the inferred isopycnal transport (V_S), calculated from the surface fluxes south of 30°S. Both $V_{ACC}(\sigma)$ and $V_S(\sigma)$ are northward in the thermocline/IW waters and southward in the upper- and deep-water layers. However, quantitatively, the actual and inferred isopycnal transports are very different. For instance, the minimum of the actual circulation $V_{ACC}(\sigma)$ occurs at $\sigma = 27.5$, whereas $V_S(\sigma)$ reaches the minimum at $\sigma = 27.2$. Note that in the absence of the diapycnal fluxes in the ACC, V_{ACC} and V_S would be equal. Thus, considerable differences between the two point to the importance of diabatic processes in the Southern Ocean.

The difference between V_{ACC} and V_S is consistent with that between the inferred and actual overturning in Fig. 5. In both cases, substantial differences occur at $\sigma = 27.2$–27.5, and the patterns of the mismatch are very similar. Therefore, we conclude that the enhanced diapycnal fluxes in the ACC, evident in Fig. 9, also project on the difference between global V_a and V_{eq}. The most notable consequence of this diabatic contamination of V_{eq} in the Southern Ocean is the shift in the lower boundary of the northward-flowing intermediate water toward heavier densities (Fig. 5), from $\sigma = 27.2$ to $\sigma = 27.5$.

The proposed connection between the diapycnal fluxes in the Southern Ocean and mismatch between V_a and V_{eq} becomes even more apparent in the following diagnostics. We construct the new generalized push–pull mode $V_a^{(g)}$ by confining our analysis to the latitudes north of 30°S. In each density layer, meridional transport at 30°S is directly diagnosed from the GCM, incorporated in $V_S(\sigma)$, and the push–pull mode is then constructed using (11). Thus, the generalized push–pull mode explicitly excludes the ACC—differences between $V_a^{(g)}$ and V_{eq} are now caused only by the diapycnal fluxes north of 30°S. This change in the definition of the push–pull mode dramatically improved its agreement with the actual transport. The resulting $V_a^{(g)}$ (Fig. 10) is very similar to V_{eq} for $26 < \sigma < 27.5$, albeit a

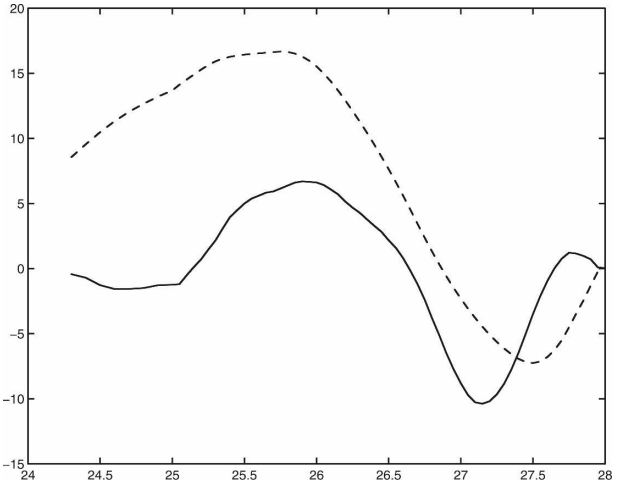

FIG. 9. Meridional transport in the Southern Ocean. The zonally integrated isopycnal volume flux (in Sv) between $\sigma_{max} = 28.0$ and σ is plotted as a function of σ. The dashed line shows the GCM-simulated transport (V_{ACC}) at 30°S; the solid line shows $V_S(\sigma)$ estimated from the surface density fluxes for the area south of 30°S.

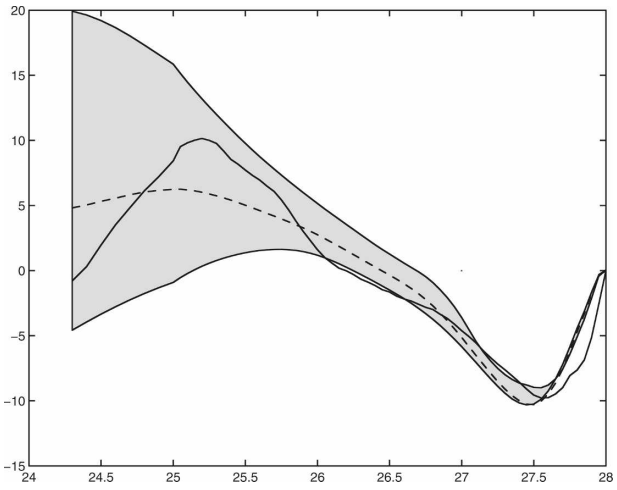

FIG. 10. Global overturning. The zonally integrated isopycnal volume flux (in Sv) between $\sigma_{\max} = 28.0$ and σ is plotted as a function of σ. The dashed line shows the GCM-simulated transport at the equator; the solid line shows the push–pull mode estimated from the surface density fluxes over the area north of 30°S plus the V_{ACC} at 30°S. Also shown are the meridional transports for 4°S (upper curve) and 4°N (lower curve); the area between these two curves is shaded.

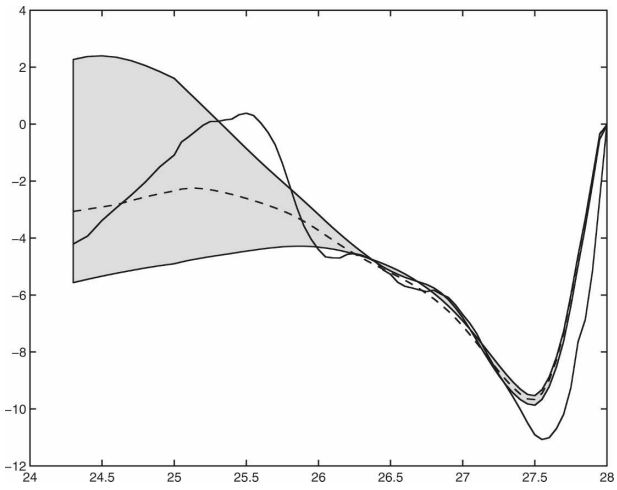

FIG. 11. Atlantic overturning. The zonally integrated isopycnal volume flux (in Sv) between $\sigma_{\max} = 28.0$ and σ is plotted as a function of σ. The dashed line shows the GCM-simulated transport at the equator; the solid line shows the push–pull mode estimated from the surface density fluxes over the area north of 30°S plus the V_{ACC} at 30°S. Also shown are the meridional transports at 4°S (upper curve) and 4°N (lower curve); the area between these two curves is shaded.

somewhat weaker southward transport for denser water masses.

Here, $V_a^{(g)}$ also diverges from V_{eq} for $\sigma < 26.0$, which is attributed to the strong diapycnal flux associated with the equatorial upwelling in the upper ocean. The equatorial upwelling is not centered exactly at the equator and, therefore, contributes to the diapycnal distortion V_{diap}. With regard to the latter issue, it should be emphasized that our decision to compare the push–pull mode with the isopycnal fluxes exactly at the equator was rather arbitrary. To give a sense of the range of the variation of isopycnal transports with latitude, in Fig. 10 we also show the transports at 4°S and 4°N; the difference is particularly large in the upper 200 m ($\sigma < 25.5$–26.0), where most of the equatorial upwelling takes place both in the model and in nature (Kessler 2006).

Similar to the global calculation, exclusion of the ACC in the Atlantic calculation (Fig. 11) improved the agreement between the push–pull mode $V_a^{(g)}$ and V_{eq} (cf. Figs. 7, 11). The $V_a^{(g)}$ and V_{eq} still differ for $\sigma >$ 27.4, a consequence of small but not negligible diapycnal fluxes north of 30°S. The push–pull mode also diverges from V_{eq} for lower densities, $\sigma < 26.0$, which we attribute to the equatorial upwelling. In the Indo-Pacific (Fig. 12), the generalized push–pull mode $V_a^{(g)}$ agrees reasonably well with V_{eq} for $\sigma > 25.5$, although weak southward transport of the deep water is not seen in $V_a^{(g)}$. The Indo-Pacific circulation is characterized by a stronger equatorial upwelling, as indicated by the variation of the transport with latitude (Fig. 12): the flow at $\sigma < 26.0$ is predominantly northward at 4°S and southward for 4°N. This upwelling adversely affects the agreement between $V_a^{(g)}$ and V_{eq} in the upper ocean. In particular, the push–pull mode in the Indo-Pacific basin bears more resemblance to the isopycnal flux at 4°N than exactly at the equator. Another source of disagreement is related to the geometry of the Indian Ocean. It is located primarily in the Southern Hemisphere, and therefore land barriers block the isopycnal meridional transport. The water masses are thereby

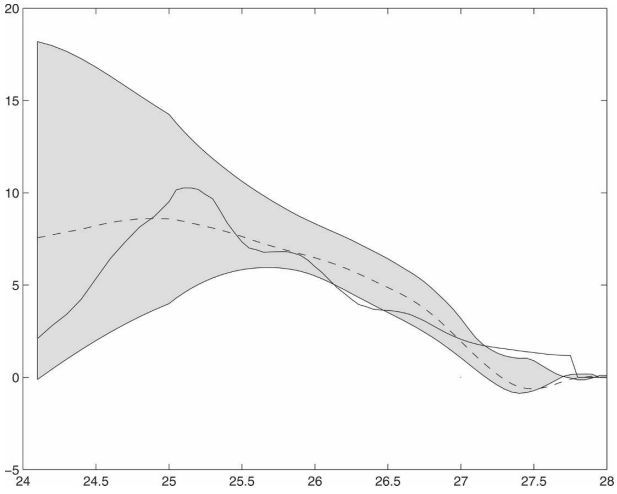

FIG. 12. Same as in Fig. 11, but for the Indo-Pacific basin.

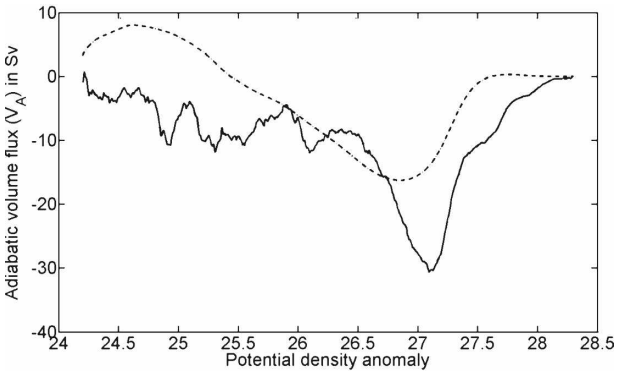

FIG. 13. The push–pull mode of the World Ocean. Solid curve presents the net isopycnal transport. Its time-mean component, directly driven by the Ekman pumping, is indicated by the dashed curve.

forced to cross the isopycnal surfaces, which greatly contributes to the diapycnal distortion V_{diap} and, ultimately, to the difference between V_{eq} and V_a.

In summary, we conclude that the differences between V_{eq} and V_a at intermediate and deep layers can be attributed, at least in the GCM, mainly to the diapycnal fluxes within the ACC. These fluxes shift the minimum in $V_a(\sigma)$, relative to $V_{\text{eq}}(\sigma)$, toward lower densities. In the upper layers, we ascribe the difference between V_{eq} and V_a to the strong, and not exactly symmetric, equatorial upwelling.

5. Application to the observed air–sea fluxes

The analysis of the GCM-simulated data prepared us for the application of our analysis to observations. However, before going on, it should be noted that there is a significant uncertainty in measurements of the air–sea fluxes, particularly over poorly sampled regions as the Southern Ocean. The estimates of the surface density flux using the existing datasets differ considerably. Here we present the results based on the surface density flux from the ECMWF reanalysis and the mixed layer density from the Levitus climatology.

a. Global overturning

The diagnostic model of section 2 is first applied to the global configuration. The analyzed density range extends from $\sigma_0 = 24.2$, the lowest density value for which the northern and southern outcrops do not intersect, to $\sigma_{\max} = 28.3$, the highest density of the ice-free sea surface area. Figure 13 shows the push–pull component (V_a) of the global MOC computed using Eq. (12). The pattern of V_a is generally consistent with the corresponding prediction of the numerical model in Fig. 5. It is characterized by a prominent minimum at $\sigma = 27.2$, which separates the northward-moving flow of the intermediate water from the dense southward-flowing deep water. The overturning estimated by Talley et al. (2003), on the other hand, suggests that the actual overturning V_{eq} changes direction at $\sigma = 27.5$. The differences between V_{eq} and V_a estimated from observations are therefore similar to those in the GCM. Southward transport of thermocline waters for $\sigma < 25.5$ in Fig. 13 is also reminiscent of a similar feature in the GCM-simulated fields (Fig. 5). The maximum global overturning of ~30 Sv is noticeably larger than the maximum overturning of ~20 Sv in the numerical model and in estimates based on the hydrographic data (Talley et al. 2003).

In an attempt to isolate the MOC component, which is driven directly by the wind stress, we also present (dashed line in Fig. 13) the estimate of the time-mean isopycnal flux ($\overline{V}_a$). A natural way to isolate $\overline{V}_a$ is related to our definition (11) of the push–pull mode in terms of the subduction rates at the northern and southern outcrops (V_S, V_N). The V_S and V_N, in turn, can be separated into the time-mean components ($\overline{V}_S$, $\overline{V}_N$) and the remaining eddy-induced transport, and therefore the time-mean push–pull mode is defined as

$$\overline{V}_a(\sigma) = \frac{1}{2}[\overline{V}_S(\sigma) - \overline{V}_N(\sigma)]. \tag{17}$$

Assuming that ($\overline{V}_S$, $\overline{V}_N$) are dominated by the Ekman divergence, we express them as

$$\overline{V}_N(\sigma) = \iint\limits_{\substack{\sigma_{\max}<\sigma'<\sigma \\ \text{north}}} w_{\text{Ek}}\, dS \approx -\int\limits_{\substack{\sigma \\ \text{north}}} \frac{1}{\rho}\mathbf{M}_{\text{Ek}} \cdot \mathbf{n}\, dl,$$

$$\overline{V}_S(\sigma) = \iint\limits_{\substack{\sigma_{\max}<\sigma'<\sigma \\ \text{south}}} w_{\text{Ek}}\, dS \approx -\int\limits_{\substack{\sigma \\ \text{south}}} \frac{1}{\rho}\mathbf{M}_{\text{Ek}} \cdot \mathbf{n}\, dl, \tag{18}$$

where $\mathbf{M}_{\text{Ek}} = [-(\tau_y/f), (\tau_x/f)]$ is the Ekman flux. Data for the wind stress are also taken from the ECWMF reanalysis, and $\overline{V}_a$ is evaluated using (17) and (18). Figure 13 indicates that while distribution of V_a and $\overline{V}_a$ differ in details—to be expected in view of considerable eddy transports and perhaps even larger observational errors—the bulk measures of the estimated mean and residual circulation are mutually consistent. The $\overline{V}_a(\sigma)$ is characterized by a minimum at $\sigma = 26.9$, only slightly shifted toward the lighter densities relative to the minimum of $V_a(\sigma)$. The maximum mean overturning, computed as a difference between the maximum and minimum of the curve in Fig. 13, is ~30 Sv, which is comparable to that of the net, mean, and eddy-induced

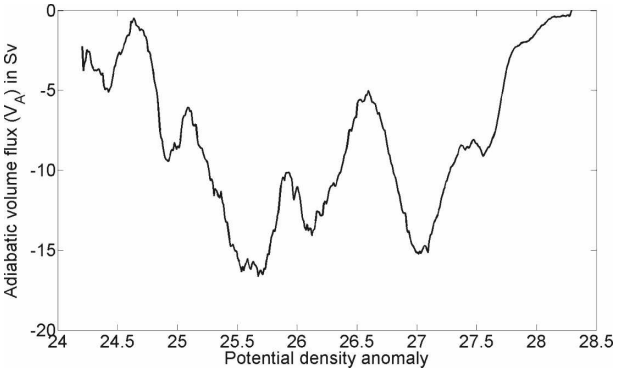

FIG. 14. The inferred isopycnal flux in the Atlantic.

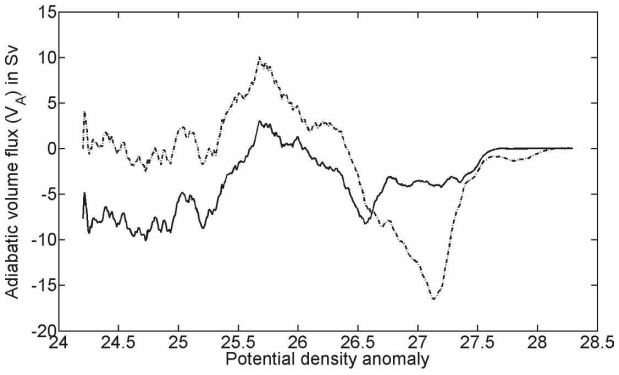

FIG. 15. Inferred isopycnal transport in the Pacific (solid curve) and Indo-Pacific (dashed–dotted curve).

transport. However, the mean transport is systematically offset from V_a by an average of 7 Sv. The general similarity of patterns of the total and mean fluxes suggests that the MOC is influenced by the difference in strengths of the Ekman pumping in the Southern and Northern Hemispheres over the corresponding (in terms of density range) surface areas.

b. *Partitioning of the global transport between the basins*

The Atlantic basin (see Fig. 1a) is characterized by $\sigma_{\max} = 28.3$ and $\sigma_0 = 24.2$. The isopycnal flux V_a is shown in Fig. 14, and we assume that the water mass budget is affected by the inflow and outflow of the ACC only in the density range of $27.3 < \sigma < 28.0$ (Fig. 6). The southward flux of the North Atlantic Deep Water is reflected in the increase in V_a by 15 Sv from $\sigma = 27$ to $\sigma = 28.3$. The northward-moving water masses originating in the ACC—the Antarctic Intermediate Water and the Subantarctic Mode Water—also have a clear signature associated with the decrease in V_a by 10 Sv from $\sigma = 26.5$ to $\sigma = 27$.

There is a second minimum of the isopycnal transport within the range $25.3 < \sigma < 25.8$, which is attributed to the extreme cooling in the Gulf Stream. This heat loss is associated with the poleward flow in the mixed layer, which is accompanied by the equivalent equatorward interior transport. Because this extreme cooling is limited to the very narrow Gulf Stream region, it may not be adequately captured by coarse-resolution observations and models. Therefore, the second minimum of $V_a(\sigma)$ at $\sigma = 25.5$ is less robust. Our experiments with other databases (not shown) indicate that the magnitude of the second minimum strongly varies between datasets; in the ECMWF reanalysis, it is likely to be exaggerated. The average diapycnal transport (RMS V_d), computed using (7), is 7 Sv, which is considerably less than the magnitude of the push–pull mode $V_a \sim 15$ Sv. This result supports the view that the adiabatic processes, advection and eddy-transfer, control the meridional overturning in the Atlantic thermocline. Comparison of Fig. 14 with the corresponding global diagnostics in Fig. 13 indicates that the global pole-to-pole MOC is controlled by the Atlantic contribution.

Figure 15 presents the push–pull modes for the Pacific (solid curve) and combined Indo-Pacific (dashed–dotted curve) basins. The Pacific push–pull mode exhibits a northward flow of 8 Sv for densities $25.7 < \sigma < 26.5$, which is somewhat stronger than in the estimates based on hydrographic data (Talley et al. 2003). The southward flow along the deeper isopycnals in the push–pull mode is similar in magnitude to that in Talley et al. The inclusion of the Indian Ocean in our analysis (dashed–dotted line in Fig. 15) increases the net overturning; the southward flux of the deep water and the northward flux of the intermediate water both amplify considerably. However, the pattern and magnitude of the transport of the thermocline waters ($\sigma < 26$) is apparently controlled by the Pacific.

6. Discussion and conclusions

The oceanic meridional overturning circulation (MOC) is accompanied by the diabatic transformation of the water masses and interacts with the air–sea buoyancy fluxes (Walin 1982). The two major mechanisms for water mass transformation are the interior diapycnal diffusion and the diabatic processes in the upper mixed layer. Their relative importance is uncertain and much debated. Our work may help to resolve this dispute by relating the major characteristics of the MOC to the subduction from the upper mixed layer. As indicated in the schematic diagram in Fig. 3b, each density layer can be thought of as a "leaky pipe" connecting the two hemispheres that is "pumped" at its two ends with different forces. We argue that this difference in pump-

ing ultimately determines the direction and the average transport of the flow, although a certain amount of water "leaks" in the interior due to diabatic processes. This conceptual view has been expressed (Radko 2007) in a recent idealized model of the pole-to-pole MOC, which confines all diabatic processes to the upper mixed layer. The analytical solutions in Radko (2007) represent the overturning circulation set up by the interplay between the winds and surface buoyancy distribution; its plausible magnitude (~10 Sv) implies that it is indeed possible to maintain the MOC even in the absence of the interior mixing.

In the present paper, we go further to explore the connection between the MOC and the pattern of the air–sea fluxes. We identify the component of the total isopycnal transport that is driven directly by the subduction from the mixed layer (the push–pull mode) and propose an efficient method for reconstructing it from the sea surface data. The application of the diagnostic theory to the GCM-simulated ocean state produced encouraging results. We show that the push–pull mode is similar, in terms of the magnitude and pattern, to the actual interhemispheric transport in the model. They are mutually consistent in terms of predicting the net interhemispheric transport in the main thermocline, globally and in the individual basins (see Table 1), and the agreement is particularly good for the Atlantic. Our findings thereby underscore the importance of the adiabatic processes, isopycnal advection and eddy transfer for the dynamics of the MOC. The remaining differences between the inferred and actual transports are attributed to the asymmetries in the distribution of the diapycnal fluxes with respect to the equator. We find that this asymmetry is largely caused by the elevated (both in models and in nature) diapycnal mixing in the Southern Ocean.

While our numerical tests are suggestive with regard to the significance of the push–pull mechanism of the interhemispheric transport, the proposed diagnostic model should be applied to the oceanic data with caution. Strictly speaking, the push–pull mode equals the actual isopycnal transport at the latitude that separates an ocean basin into two parts with equal diapycnal mass transport. We have assumed that this latitude is located somewhere in the vicinity of the equator. However, our analysis indicates that the asymmetries in diabatic processes across the equator are nonnegligible and lead to the difference between the push–pull mode and the interhemispheric transport. The distribution of the diapycnal fluxes in the ocean is not well known and, furthermore, can be substantially different from that in the numerical models. Thus, one cannot exclude the possibility that the fraction of the net MOC driven by the push–pull mechanism in the ocean could be less than in our model-based estimates. This possibility, however, seems unlikely because most of the coarse-resolution models are known to exaggerate (rather than underestimate) the strength of diabatic processes.

Application of the proposed technique to the ECMWF air–sea fluxes also resulted in plausible values and patterns of the MOC characterized by the southward transport of deep waters and the northward return flow in the main thermocline. The major features of the inferred overturning are generally consistent with the estimates based on in situ temperature and horizontal velocity measurements (Talley et al. 2003) for the Atlantic and Pacific Oceans. The qualitative agreement lends further credence to the idea that the interhemispheric transport is strongly influenced, perhaps even controlled, by the adiabatic push–pull mechanism.

Finally, we wish to mention that generally the application of the water mass transformation theory to the sea surface observational data is greatly restricted by the observational uncertainties—the air–sea fluxes in various datasets differ by as much as a factor of 2 or more. However, these uncertainties affect the push–pull mode (V_a) not nearly as severely as the diapycnal flux (V_d). Our estimate of V_a is based on the difference between the air–sea fluxes at the northern and southern outcrops of each isopycnal surface. Therefore, our method results in a partial cancellation of the systematic errors in flux measurements. In addition to the ECMWF dataset discussed in our paper, we have examined National Centers for Environmental Prediction (NCEP), Southampton Oceanography Centre Global Air–Sea heat and momentum flux (SOC-GAS97), and Da Silva sets Da Silva et al. (1994) and found that they are consistent in terms of reconstructing the push–pull mode (V_a). They predict the global V_a with a standard deviation of 6.7 Sv, which is by far less than 32.1 Sv for the diapycnal MOC component.

Acknowledgments. The authors thank John Marshall, Lynne Talley, and reviewers for helpful comments. TR acknowledges support by the National Science Foundation (Grant OCE 0623524); IK was supported by the National Science Foundation (Grant OCE 0623608) and National Aeronautics and Space Administration (Grant NNG06GA66G).

APPENDIX

Subduction from the Mixed Layer in the Eddying Ocean

It has been long recognized (Andrews and McIntyre 1976) that the distribution of buoyancy and tracers in

eddying flows cannot be accounted for by the Eulerian mean circulation, but also involves the eddy-induced advection, a process similar to the Stokes drift. The time-mean density equation takes into account the eddy fluxes as follows:

$$\mathbf{v} \cdot \nabla\sigma + \nabla(\overline{\mathbf{v}'\sigma'}) = \frac{\partial B}{\partial z}, \tag{A1}$$

where σ is the time-mean density anomaly and primes denote the perturbations from this mean due to transient eddies. The B represents the vertical density flux due to small-scale processes and air–sea fluxes. The eddy fluxes in (A1), which we largely associate with mesoscale variability, can be decomposed into two distinct components—adiabatic advection by the nondivergent eddy-induced velocity of the residual mean theory ($\mathbf{v}^*$) and the remaining diabatic component. The latter is written, without loss of generality, as convergence of the vertical density flux $\partial B_{\text{eddy}}/\partial z$. As a result, the density Eq. (A1) becomes

$$\mathbf{v}_{\text{res}} \cdot \nabla\sigma = \frac{\partial \tilde{B}}{\partial z}, \tag{A2}$$

where the residual velocity $\mathbf{v}_{\text{res}} = \mathbf{v} + \mathbf{v}^*$ represents the advection of buoyancy and tracers by both mean field and adiabatic eddies, and $\tilde{B} = B + B_{\text{eddy}}$ includes diabatic effects of the small-scale mixing and eddies.

Following Marshall and Radko (2003), we separately discuss dynamics of the thin, vertically homogeneous mixed layer ($-h_m < z < 0$) and the stratified interior ($z < -h_m$). In the mixed layer, the residual buoyancy equation reduces to

$$u_{\text{res}} \frac{\partial \sigma_m}{\partial x} + \mathbf{v}_{\text{res}} \frac{\partial \sigma_m}{\partial y} = \frac{\partial \tilde{B}}{\partial z}, \tag{A3}$$

where σ_m is the mixed layer density. Integration of (A3) over the depth of the mixed layer results in

$$U \frac{\partial \sigma_m}{\partial x} + V \frac{\partial \sigma_m}{\partial y} = B_0 + B_{\text{mle}} - \tilde{B}\big|_{z=-h_m}, \tag{A4}$$

where $U = \int_{-h_m}^{0} u_{\text{res}}\, dz$, $V = \int_{-h_m}^{0} \text{v}_{\text{res}}\, dz$, B_0 is the air–sea density flux, B_{mle} is a contribution from the diabatic eddies in the mixed layer, and $\tilde{B}|_{z=-h_m}$ is the vertical density flux due to diabatic processes immediately below the mixed layer.

In the mixed layer density Eq. (A4), the total density flux on its right-hand side is dominated by the direct air–sea forcing B_0. The estimates in Radko and Marshall (2006), in the context of the ACC, suggest that the sea surface flux B_0 exceeds B_{mle} by an order of magnitude. The diabatic eddy fluxes play an even lesser role on planetary scales (e.g., Radko 2007)—the primary focus of this study. Thus, the B_{mle} term in (A4) is neglected, an approximation that presumably contributes to the error of our diagnostic model but greatly simplifies the analytical development. We note, however, that the neglect of B_{mle} in this particular balance should not be interpreted as a statement that the lateral eddy fluxes in the mixed layer are unimportant in general. Examples of their significance include the study of Greatbatch et al. (2007), who argued that the mixed layer eddies may be critical in balancing the heat budget of the upper ocean.

Below the mixed layer, both small-scale mixing and the diabatic eddy effects are greatly reduced, and therefore $B_0 \gg \tilde{B}|_{z=-h_m}$. Thus, Eq. (A4) is approximated by

$$U \frac{\partial \sigma_m}{\partial x} + V \frac{\partial \sigma_m}{\partial y} = B_0, \tag{A5}$$

and more concisely written as

$$\mathbf{U} \cdot \mathbf{n} = \frac{B_0}{|\nabla\sigma_m|}, \tag{A6}$$

where $\mathbf{n} = (\nabla\sigma_m)/|\nabla\sigma_m|$ is the unit vector normal to the buoyancy contours. Consider now a strip of fluid bounded by two nearby surface isopycnals (σ and $\sigma + \Delta\sigma$) as indicated in the schematic in Fig. 2. The net volume flux into the mixed layer over its area (δS) is given by

$$\delta V = \iint_{\delta S} W\, dS, \tag{A7}$$

where $W = w_{\text{res}}|_{z=-h_m} + (u_{\text{res}}, \upsilon_{\text{res}}) \cdot \nabla h_m$ is the volume flux per unit area.

The area of integration in (A7) extends from one intersection with the coastal boundary to another if the buoyancy contours are blocked by the land, and it may include contributions from several ocean basins. For closed surface density contours (these exist in, e.g., the reentrant Antarctic Circumpolar Current), the integral pertains to the entire simply connected area between contours σ and $\sigma + \Delta\sigma$. To evaluate the integral in (A7), we assume no flux across the coastal boundaries for zonally blocked flows or the exact cancellation of zonal fluxes in case of a reentrant flow. We also assume that the residual transport, sum of the mean and eddy induced, does not penetrate across the surface of the ocean. Therefore, the integrated vertical residual flux at the bottom of the mixed layer is equal to the sum of the lateral residual fluxes into the area bounded by contours σ and $\sigma + \Delta\sigma$ (see Fig. 2):

$$\iint_{\delta S} W\, dS = \int_{\sigma+\Delta\sigma} \mathbf{U} \cdot \mathbf{n}\, dl - \int_{\sigma} \mathbf{U} \cdot \mathbf{n}\, dl, \tag{A8}$$

where l is the arc length along the mixed layer density contours.[A1] Taking the limit $\Delta\sigma \to 0$ and using (A6), we rewrite (A8) as

$$\iint_{\delta S} W\, dS = \frac{\partial}{\partial \sigma}\left(\int_{\sigma} \frac{B_0}{|\nabla \sigma_m|}\, dl\right) \cdot \Delta\sigma. \qquad \text{(A9)}$$

The line integral in $\int_\sigma (B_0/|\nabla\sigma_m|)\, dl$ can be transformed into the area integral and cast in the familiar Walin's form:

$$\int_{\sigma} \frac{B_0}{|\nabla \sigma_m|}\, dl = \frac{\partial}{\partial \sigma} \iint_{S(\sigma)} B_0\, dS = F(\sigma), \qquad \text{(A10)}$$

where integration is carried over the surface area bounded by the mixed layer density contour σ and some reference surface isopycnal with lower density located in the same hemisphere, and F is the water mass transformation function.

REFERENCES

Andrews, D. G., and M. E. McIntyre, 1976: Planetary waves in horizontal and vertical shear: The generalized Eliassen–Palm relation and the mean zonal acceleration. *J. Atmos. Sci.,* **33,** 2031–2049.

Boccaletti, G., R. Ferrari, A. Adcroft, D. Ferreira, and J. Marshall, 2005: The vertical structure of the ocean heat transport. *Geophys. Res. Lett.,* **32,** L10603, doi:10.1029/2005GL022474.

Bryan, K., and L. J. Lewis, 1979: A water mass model of the world ocean. *J. Geophys. Res.,* **84,** 2503–2517.

Cerovečki, I., and J. Marshall, 2008: Eddy modulation of air–sea interaction and convection. *J. Phys. Oceanogr.,* **38,** 65–83.

Da Silva, A., A. C. Young, and S. Levitus, 1994: *Algorithms and Procedures.* Vol. 1, *Atlas of Surface Marine Data*, NOAA Atlas NESDIS 1, 83 pp.

Donners, J., S. S. Drijfhout, and W. Hazeleger, 2005: Water mass transformation and subduction in the South Atlantic. *J. Phys. Oceanogr.,* **35,** 1841–1860.

Garrett, C., and A. Tandon, 1997: The effects on water mass formation of surface mixed layer time-dependence and entrainment fluxes. *Deep-Sea Res. I,* **44,** 1991–2006.

——, K. Speer, and E. Tragou, 1995: The relationship between water mass formation and the surface buoyancy flux, with application to Phillip's Red Sea model. *J. Phys. Oceanogr.,* **25,** 1696–1705.

Gent, P. R., and J. C. McWilliams, 1990: Isopycnal mixing in ocean circulation models. *J. Phys. Oceanogr.,* **20,** 150–155.

Gnanadesikan, A., 1999: A simple predictive model for the structure of the oceanic pycnocline. *Science,* **283,** 2077–2079.

Greatbatch, R. J., X. Zhai, C. Eden, and D. Olbers, 2007: The possible role in the ocean heat budget of eddy-induced mixing due to air–sea interaction. *Geophys. Res. Lett.,* **32,** L07604, doi:10.1029/2007GL029533.

Henning, C. C., and G. Vallis, 2004: The effects of mesoscale eddies on the main subtropical thermocline. *J. Phys. Oceanogr.,* **34,** 2428–2443.

Kamenovich, I. V., 2005: Role of daily surface forcing in setting the temperature and mixed layer structure of the Southern Ocean. *J. Geophys. Res.,* **110,** C07006, doi:10.1029/2004JC002610.

Karsten, R., and J. Marshall, 2002: Constructing the residual circulation of the ACC from observations. *J. Phys. Oceanogr.,* **32,** 3315–3327.

Kessler, W. S., 2006: The circulation of the eastern tropical Pacific: A review. *Prog. Oceanogr.,* **69,** 181–217.

Large, W. G., J. C. McWilliams, and S. C. Doney, 1994: Oceanic vertical mixing: A review and a model with a nonlocal boundary layer parameterization. *Rev. Geophys.,* **32,** 363–403.

Luyten, J., J. Pedlosky, and H. Stommel, 1983: The ventilated thermocline. *J. Phys. Oceanogr.,* **13,** 292–309.

Marshall, D., 1997: Subduction of water masses in an eddying ocean. *J. Mar. Res.,* **55,** 201–222.

Marshall, J., and T. Radko, 2003: Residual-mean solutions for the Antarctic Circumpolar Current and its associated overturning circulation. *J. Phys. Oceanogr.,* **33,** 2341–2354.

——, and ——, 2006: A model of the upper branch of the meridional overturning of the southern ocean. *Prog. Oceanogr.,* **70,** 331–345.

——, D. Jamous, and J. Nilsson, 1999: Reconciling thermodynamic and dynamic methods of computation of water-mass transformation rates. *Deep-Sea Res. I,* **46,** 545–572.

——, H. Jones, R. Karsten, and R. Wardle, 2002: Can eddies set ocean stratification? *J. Phys. Oceanogr.,* **32,** 26–38.

Munk, W., 1966: Abyssal recipes. *Deep-Sea Res.,* **13,** 707–730.

Olbers, D., D. Borowski, C. Volker, and J. O. Wolff, 2004: The dynamical balance, transport and circulation of the Antarctic Circumpolar Current. *Antarct. Sci.,* **16,** 439–470.

Pacanowski, R. C., and S. M. Griffies, 1999: MOM 3.0 manual: Documentation, user's guide, and reference manual. NOAA/Geophysical Fluid Dynamics Laboratory, 668 pp.

Polzin, K. L., J. M. Toole, J. R. Ledwell, and R. W. Schmitt, 1997: Spatial variability of turbulent mixing in the abyssal ocean. *Science,* **276,** 93–96.

Radko, T., 2007: A mechanism for establishment and maintenance of the meridional overturning in the upper ocean. *J. Mar. Res.,* **65,** 85–116.

——, and J. Marshall, 2004: Eddy-induced diapycnal fluxes and their role in the maintenance of the thermocline. *J. Phys. Oceanogr.,* **34,** 372–383.

——, and ——, 2006: The Antarctic Circumpolar Current in three dimensions. *J. Phys. Oceanogr.,* **36,** 651–669.

Robinson, A. R., and H. Stommel, 1959: The oceanic thermocline and the associated thermohaline circulation. *Tellus,* **11,** 295–308.

Salmon, R., 1990: The thermocline as an "internal boundary layer." *J. Mar. Res.,* **48,** 437–469.

Samelson, R. M., and G. K. Vallis, 1997: Large-scale circulation with small diapycnal diffusion: The two-thermocline limit. *J. Mar. Res.,* **55,** 223–275.

Sloyan, B. M., and S. R. Rintoul, 2000: Estimates of area-averaged

[A1] While the schematic in Fig. 2 and the related discussion represents the case in which density increases northward (the configuration relevant for the Northern Hemisphere), it can be easily shown that our formulation applies to both Northern and Southern Hemispheres.

diapycnal fluxes from basin-scale budgets. *J. Phys. Oceanogr.,* **30,** 2320–2341.

Speer, K., and E. Tziperman, 1992: Rates of water mass formation in the North Atlantic Ocean. *J. Phys. Oceanogr.,* **22,** 93–104.

——, H.-J. Isemer, and A. Biastoch, 1995: Water mass formation from revised COADS data. *J. Phys. Oceanogr.,* **25,** 2444–2457.

——, S. R. Rintoul, and B. Sloyan, 2000: The diabatic Deacon cell. *J. Phys. Oceanogr.,* **30,** 3212–3222.

Talley, L. D., 2003: Shallow, intermediate, and deep overturning components of the global heat budget. *J. Phys. Oceanogr.,* **33,** 530–560.

——, J. L. Reid, and P. E. Robbins, 2003: Data-based meridional overturning streamfunctions for the global ocean. *J. Climate,* **16,** 3213–3226.

Tandon, A., and K. Zahariev, 2001: Quantifying the role of mixed layer entrainment for water mass transformation in the North Atlantic. *J. Phys. Oceanogr.,* **31,** 1120–1131.

Timmermann, A., and H. Goosse, 2004: Is the wind stress forcing essential for the meridional overturning circulation? *Geophys. Res. Lett.,* **31,** L04303, doi:10.1029/2003GL018777.

Toggweiler, J. R., and B. Samuels, 1998: On the ocean's large-scale circulation near the limit of no vertical mixing. *J. Phys. Oceanogr.,* **28,** 1832–1852.

Trenberth, K. E., and J. M. Caron, 2001: Estimates of meridional atmosphere and ocean heat transports. *J. Climate,* **14,** 3433–3443.

Tziperman, E., 1986: On the role of interior mixing and air–sea fluxes in determining the stratification and circulation of the oceans. *J. Phys. Oceanogr.,* **16,** 680–693.

Walin, G., 1982: On the relation between sea-surface heat flow and thermal circulation in the ocean. *Tellus,* **34,** 187–195.

Webb, D. J., and N. Suginohara, 2001: Vertical mixing in the ocean. *Nature,* **409,** 37.

Welander, P., 1986: Thermohaline effects in the ocean circulation and related simple models. *Large-Scale Transport Processes in Oceans and Atmosphere,* J. Willebrand and D. L. T. Anderson, Eds., D. Reidel, 163–200.

Whitehead, J. A., 1995: Thermohaline ocean processes and models. *Annu. Rev. Fluid Mech.,* **27,** 89–113.

Wunsch, C., and R. Ferrari, 2004: Vertical mixing, energy, and the general circulation of the oceans. *Annu. Rev. Fluid Mech.,* **36,** 281–314.